Aerosol Science and Technology

ISSN: 0278-6826 (Print) 1521-7388 (Online) Journal homepage: http://www.tandfonline.com/loi/uast20

Laboratory Evaluation and Calibration of Three Low-Cost Particle Sensors for Particulate Matter Measurement

Yang Wang, Jiayu Li, He Jing, Qiang Zhang, Jingkun Jiang & Pratim Biswas

To cite this article: Yang Wang, Jiayu Li, He Jing, Qiang Zhang, Jingkun Jiang & Pratim Biswas (2015) Laboratory Evaluation and Calibration of Three Low-Cost Particle Sensors for Particulate Matter Measurement, Aerosol Science and Technology, 49:11, 1063-1077, DOI: 10.1080/02786826.2015.1100710

To link to this article: https://doi.org/10.1080/02786826.2015.1100710

Aerosol Science and Technology, 49:1063–1077, 2015

ISSN: 0278-6826 print / 1521-7388 online
DOI: 10.1080/02786826.2015.1100710

Laboratory Evaluation and Calibration of Three Low-Cost Particle Sensors for Particulate Matter Measurement

Yang Wang,[1] Jiayu Li,[1] He Jing,[1] Qiang Zhang,[2] Jingkun Jiang,[2] and Pratim Biswas[1]
[1]*Aerosol and Air Quality Research Laboratory, Department of Energy, Environmental & Chemical Engineering, Washington University in St. Louis, St. Louis, Missouri, USA*
[2]*State Key Joint Laboratory of Environment Simulation and Pollution Control, School of Environment, Tsinghua University, Beijing, China*

Particle sensors offer significant advantages of compact size and low cost, and have recently drawn great attention for usage as portable monitors measuring particulate matter mass concentrations. However, most sensor systems have not been thoroughly evaluated with standardized calibration protocols, and their data quality is not well documented. In this work, three low-cost particle sensors based on light scattering (Shinyei PPD42NS, Samyoung DSM501A, and Sharp GP2Y1010AU0F) were evaluated by calibration methods adapted from the US EPA 2013 Air Sensor Workshop recommendations. With a SidePak (TSI Inc., St. Paul, MN, USA), a scanning mobility particle sizer (TSI Inc.), and an AirAssure™ $PM_{2.5}$ Indoor Air Quality Monitor (TSI Inc.), which itself relies on a GP2Y1010AU0F sensor as reference instruments, six performance aspects were examined: linearity of response, precision of measurement, limit of detection, dependence on particle composition, dependence on particle size, and relative humidity and temperature influences. This work found that: (a) all three sensors demonstrated high linearity against SidePak measured concentrations, with R^2 values higher than 0.8914 in the particle concentration range of 0–1000 $\mu g/m^3$, and the linearity depended on the studied range of particle concentrations; (b) the standard deviations of the sensors varied from 15 to 90 $\mu g/m^3$ for a concentration range of 0–1000 $\mu g/m^3$; (c) the outputs of all three sensors depended highly on particle composition and size, resulting in as high as 10 times difference in the sensor outputs; and (d) humidity affected the sensor response. This article provides further recommendations for applications of the three tested sensors.

1. INTRODUCTION

Particulate matter (PM) is an important parameter in determining air quality, affecting visibility (Guo et al. 2014), human health (Biswas and Wu 2005; Karlsson et al. 2009), and global climate (Stocker et al. 2013). The size of PM is closely related to the inhalation and deposition properties of particles in the human respiratory system (Phalen et al. 1991). PM concentration can be quantified as PM_{10}, $PM_{2.5}$, or PM_1, according to the mass concentrations of particles below the aerodynamic sizes of 10 μm, 2.5 μm, and 1 μm, respectively. The US EPA-approved instruments for measuring PM concentrations include impactors, cyclones, tapered element oscillating microbalances (TEOM), and beta attenuation monitors (BAM) (EPA 2013). Other instruments, such as the DustTrak™ and SidePak™ (TSI Inc., St. Paul, MN, USA) use light scattering to obtain particle mass concentrations, while scanning mobility particle sizers (SMPS; Knutson and Whitby 1975; Wang and Flagan 1990) and aerodynamic particle sizer (APS) derive particle mass concentrations from measured particle size distributions.

Temporal and spatial PM aggregate concentrations may vary significantly in a region. The PM concentrations provided by a single monitoring site may not accurately represent the particle concentrations around people distributed in its vicinity, who may be concerned about the health effects of PM exposure. In recent years, this concern has become especially acute in developing countries that are industrializing (Cao et al. 2013; Tiwari et al. 2013; Huang et al. 2014). To keep the citizens updated on air quality information through additional sources, the US embassy and consulates have started to measure and post the real-time PM concentrations in these countries. However, the embassy websites also emphasize that, "citywide analysis cannot be done, on data from a single machine (US Embassy 2015)." In order to obtain accurate PM concentrations with good resolution, a high density of measurement sites is required, and the cost associated with the conventional instruments mentioned above makes this impractical. Based on techniques first developed for smoke detectors decades ago (Mulholland and Liu 1980), portable PM monitors have become popular in recent years (Hagler et al. 2014), driven by their remarkably low price and the emerging need

Received 10 May 2015; accepted 7 September 2015.
Address correspondence to Pratim Biswas, Aerosol and Air Quality Research Laboratory, Department of Energy, Environmental & Chemical Engineering, Washington University in St. Louis, One Brookings Drive, Campus Box 1180, St. Louis, MO 63130, USA. E-mail: pbiswas@wustl.edu
Color versions of one or more of the figures in the article can be found online at www.tandfonline.com/uast.

for real-time "big data" reporting of local air quality (Chong and Kumar 2003; Leavey et al. 2015). These particle sensors can be used in locating pollution hotspots or generating coarse three-dimensional (3D) maps of PM concentrations (Rajasegarar et al. 2014). In a broader sense, the usage of low-cost particle sensors also raises social awareness of air quality.

Particle sensors using light scattering are cheaper and more compact than sensors using the single particle counting method or other mechanical methods, and hence have drawn more attention from researchers in recent years (Weekly et al. 2013; Holstius et al. 2014). A light scattering PM sensor is typically composed of an infrared emitting diode (IRED), a phototransistor (PT), and focusing lenses. While passing through the sensor, particles scatter light and the intensity of the light received by the phototransistor is directly correlated with the concentration of particles. The light scattering of particles falls into different regimes (Friedlander 2000), and the Rayleigh regime and Mie regime are often encountered for particles in micrometer size or smaller. Compared to sensors using single particle counting techniques, light scattering PM sensors measure the optical properties of the particles as an ensemble. This feature greatly reduces the cost and size of the sensors; however, at the same time, it limits their measurement accuracy (Holstius et al. 2014; Gao et al. 2015).

Three models of light scattering particle sensors, the PPD42NS (Shinyei Inc.), DSM501A (Samyoung Inc.), and GP2Y1010AU0F (Sharp Inc.) are currently available to customers as single modules, which are simple to assemble, install, and use. Each sensor has been evaluated separately in previous work, and a qualitative match was observed between their outputs and the total mass concentrations obtained by established instruments (Nafis 2012; Olivares et al. 2012; Weekly et al. 2013; Holstius et al. 2014; Gao et al. 2015). Further experiments were conducted on deploying the particle sensors for correlation with gas sensors (Olivares et al. 2012), monitoring occupancy in public space (Weekly et al. 2013), and measuring particle concentrations in field tests (Holstius et al. 2014; Gao et al. 2015). The PPD42NS sensor and GP2Y1010AU0F sensor have also been packaged in commercialized particle monitors, such as the AirAssure $PM_{2.5}$ Indoor Air Quality Monitor (TSI Inc.), which was tested in this study, the Air Box^{TM} (Haier Inc.), and the Pervasive Air-Quality Monitor (PAM, Air-Scientific). To fulfill the need for smaller, cheaper, and more accurate particle monitors, other sensors have also been designed (Litton et al. 2004; Chowdhury et al. 2007), calibrated (Edwards et al. 2006), and applied in field studies (Chowdhury et al. 2007; Sahu et al. 2011).

Up until now, no parallel comparison among these sensors has been conducted. At the same time, the lack of studies using a standard protocol assessing the particle sensors has hindered a comprehensive understanding of their performance. Several calibration protocols have been designed and used to calibrate air quality sensors (Spinelle et al. 2013; Long et al. 2014). The 2013 US EPA Air Sensor Workshop recommended seven parameters to be investigated upon the receipt of a new air quality sensor device from its developer or manufacturer: (1) linearity of response, (2) precision of measurements, (3) limit of detection, (4) concentration resolution, (5) response time, (6) interference equivalents, and (7) relative humidity (RH) and temperature influences. Among these parameters, concentration resolution is reflected in the precision of measurements, as introduced in the EPA workshop summary (Long et al. 2014). For particle sensors using light scattering method, the light transfer time in the sensors can be ignored, and their response time is mainly determined by the electron transport time in the circuits, which can also be neglected. The interference equivalent does not need to be considered, since, unlike gas sensors, for which equivalent species can cause similar responses, particle sensors are affected by concentrations and properties of particles only. Particle composition critically affects the performance of light scattering sensors. Light scattering depends on the refractive indices of materials, while the light absorption of materials may also affect the intensity of light received by the phototransistor. The size of particles also directly influences the light scattering coefficient and absorption coefficient. Previous analyses indicated that particle mass concentrations determined by nephelometry, which is also based on light scattering, have an irreducible uncertainty of approximately $\pm 30\%$ to 40%, which is directly attributable to the natural variability of $PM_{2.5}$ aerosol parameters, including particle concentration, particle refractive index, particle size, and particle morphology (Molenar 2000). Therefore, for evaluating light scattering particle sensors, the original EPA list of seven parameters was altered. Concentration resolution, response time, and interference equivalents were dropped, and particle composition and size dependence were added.

In this study, the performance of three low-cost light scattering particle sensors was compared for the first time against commonly used instruments in air quality research, a SidePak and a SMPS. The laboratory evaluation and calibration used a revised protocol provided by the EPA 2013 Air Sensor Workshop to obtain a comprehensive understanding of sensor performance.

2. CALIBRATION PLATFORM

A calibration platform was built for testing the performance of the sensors. Detailed descriptions of the sensors, the reference instruments, the chamber, and the operating principles for the measurement are as follows.

2.1. Particle Sensors and Reference Instrument

The Shinyei PPD42NS, Samyoung DSM501A, and Sharp GP2Y1010AU0F sensors were evaluated in this work. For simplification, the three sensors are named "PPD," "DSM," and "GP2Y" in the following, respectively. The geometries, schematic diagrams, and specifications of the three sensors are

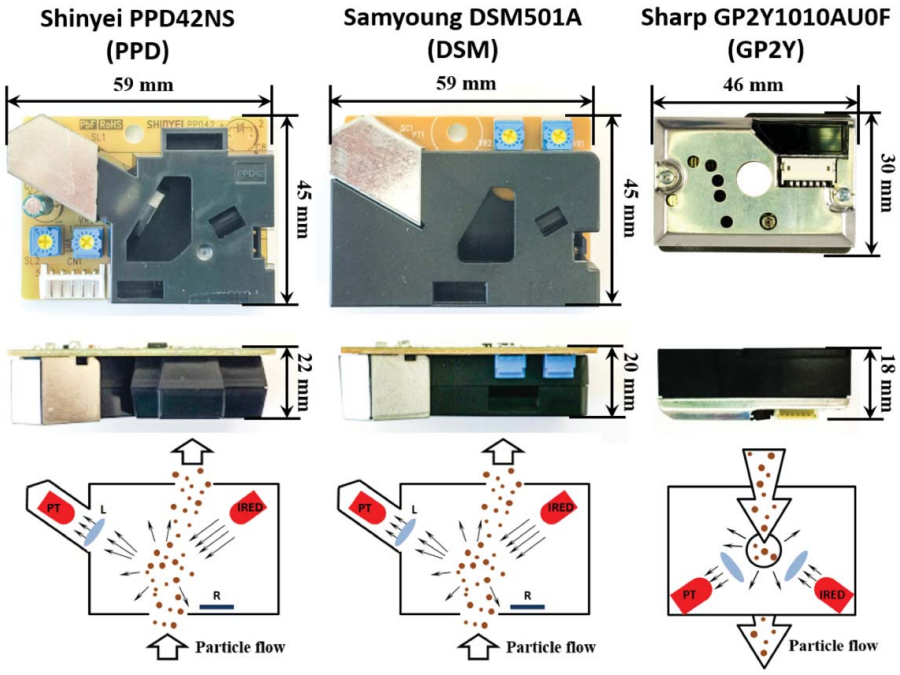

FIG. 1. Dimensions, geometries, and schematic diagrams of the sensors evaluated in this work. The sensors in the figure do not represent actual sizes. In the schematic diagrams shown in the third row, PT, IRED, and R stand for phototransistor, infrared emitting diode, and thermal resistor, respectively.

displayed in Figure 1 and Table 1. The PPD and DSM sensors share a similar geometry. Both use thermal resistors to generate heat so that natural convection creates an updraft of particles that flow through the light scattering region. The GP2Y sensor is smaller than the PPD and DSM sensors. Unlike the PPD and DSM sensors that are self-aspirated through the application of thermal resistors, the GP2Y sensor relies on a hole through the center of the body to allow for the convection of particles. The orientation of the GP2Y sensor is therefore different from the other two types of sensors, as discussed in the next section. Also, the GP2Y sensors with and without regulated external convection may respond differently under the same particle concentrations. All the tested particle sensors use IREDs for light generation, and commonly used IREDs generate light with wavelengths between 870 and 980 nm (Schubert et al. 2005).

The PPD and DSM sensors were controlled by a LabVIEW program through a data acquisition system (NI 6008, National Instruments Inc.). Both sensors output modulated pulses, whose Lo Pulse Occupancy (LPO, percentage of time during which the sensors output a low voltage in a total sampling time of 30 s) was directly correlated with the particle concentrations. Due to the need for an external high frequency square wave to trigger the diode in the sensor, the GP2Y sensor was

TABLE 1
Specifications of the tested sensors

Model	PPD42NS	DSM501A	GP2Y1010AU0F
Abbreviation used in this work	PPD	DSM	GP2Y
Dimension W × H × D (mm)	59 × 45 × 22	59 × 45 × 20	46 × 30 × 18
Detectable PM size range	~1 μm	~1 μm	N/A
Operation voltage	5 ± 0.5 V	5 ± 0.5 V	5 ± 0.5 V
Current consumption	<90 mA	<90 mA	<20 mA
Maximum detectable concentration	28,000 #/L	1400 μg/L	500 μg/m^3
Operation temperature	0 ~ +45°C	−10 ~ +65°C	−10 ~ +65°C
Operation humidity	<95%	<95%	N/A
Sensitivity	N/A	N/A	0.35–0.65 V/(100 μg/m^3)
Output signal	Pulse width modulation	Pulse width modulation	Analog output
Cost (USD)	~$15.9	~$13.8	~$10.0

connected to a programmed Arduino data acquisition board (UNO Rev 3, Arduino Inc.). The particle concentration for the GP2Y was represented by the magnitude of the output voltage. While the GP2Y has a finer time resolution for data collection, to be consistent with the PPD and DSM that have a sampling resolution of 30 s, the data for all three sensors were collected by the computer every 30 s.

A SidePak Personal Aerosol Monitor AM510 (TSI Inc.), a scanning mobility particle sizer (SMPS, TSI Inc.), and an AirAssure $PM_{2.5}$ Indoor Air Quality Monitor (TSI Inc.) were used to provide reference measurement results to evaluate the performance of the sensors. Like the sensors, the SidePak also uses light scattering, while the flow of particles is regulated by a small built-in vacuum pump. A user-defined calibration factor was used to compensate for differences in the particulate materials' refractive indices. In the experiments, the calibration factor of the SidePak was set to 1.0, because the study mainly focused on the linearity and precision of the measurements, while the calibration factor could be added in data processing.

The SMPS uses a differential mobility analyzer (DMA) to classify particles as a function of electrical mobility size, and a condensation particle counter (CPC) to measure particle concentrations. A continuous particle size distribution function is obtained through data inversion, which relates particle concentration to the charging efficiency of the neutralizer, the detection efficiency of the CPC, and the transfer function of the DMA (Stolzenburg and McMurry 2008). The mass concentration is then calculated through the integration of the product of the size distribution function and particle mass of each size. If the particles follow lognormal distributions, the method of moments is a simple approach to calculate the mass concentrations (Hinds 1982), as elaborated in Section 4.4.

The AirAssure $PM_{2.5}$ Indoor Air Quality Monitor utilizes a Sharp GP2Y sensor, and regulates the flow through the sensor via a fan attached at one side of the sensor, so that particles pass through the sensor by convective flow instead of random diffusion. A specialized algorithm averages the particle concentrations over a period time to provide more accurate results. In order to study the effect of these modifications to the sensor prototype, a comparison between the GP2Y sensors without convective flow and the AirAssure monitor was conducted, focusing on the linearity of response and the precision of measurements.

2.2. Chamber for Particle Measurement

The evaluation of the particle sensors was conducted in a custom built acrylic glass chamber with dimensions of 58 × 58 × 28 cm (Figure 2a). The edges of the chamber were sealed with rubber strips to prevent the leakage of particles and provide a uniform distribution of particles. Ports with a uniform diameter of 5 mm were drilled on the walls of the chamber to allow for sampling and passing electrical leads. During the experiments, the unused ports were snugly plugged. Generated particles were introduced into the center of the chamber via a stainless steel tube. One sensor of each type was taped to each vertical side of the chamber, and the three tested sensors were attached as closely as possible to minimize the spatial differences in particle concentrations, although the concentration variance in the chamber was found to be small (Figure 2b). The PPD and DSM sensors were fixed with their backs facing the chamber wall, so that a vertical updraft of the particles could be generated. The GP2Y sensors were placed with the front panel facing the bottom of the chamber so that particles could pass through the hole in its center. In this study, due to the relatively large size of the test chamber and the limited air exchange rates, forced convection through mixing fans created an uneven distribution of particles. To maintain a uniform particle concentration at the four sides of the chamber walls, generated particles were transported mainly by random diffusion. As indicated in Figure 2b, the difference in particle concentrations at the four sides of the chamber was within 15%. This variation in particle

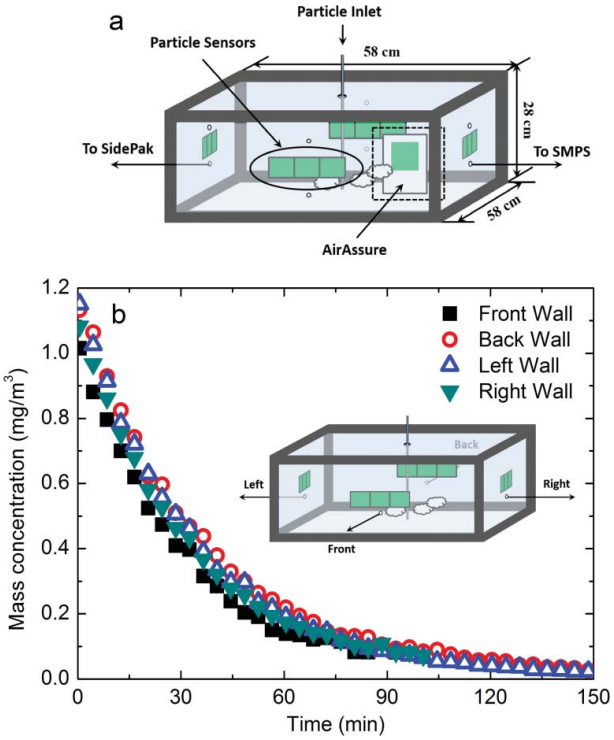

FIG. 2. (a) Schematic diagram of the chamber for particle measurement and the arrangement of particle sensors. There are two ports on each vertical side of the chamber. The upper four ports were used for passing the electrical leads. The lower four ports allowed for particle sampling, including testing the sensor performance, where two ports were used by the SidePak and the SMPS; and testing the uniformity of the particle distribution, where all the four ports were used by the SidePak (b). During the experiments, the unused ports were plugged. The AirAssure monitor (marked with a dashed box) was placed in the chamber only when comparing the performance with the GP2Y sensors without convective flow. (b) Particle mass concentrations measured from the four sides of the chamber. The results indicate that particles were uniformly distributed.

concentration might result in different outputs of the four sensors of each type, but it was not the major reason for the deviation of the response of some sensors, as discussed in Section 4.1. The SidePak and SMPS were outside the chamber, and particle streams were sampled via tubes located 2 cm below the sensors on two side walls of the chamber, at flow rates of 0.7 lpm and 0.3 lpm, respectively. The AirAssure monitor was not placed in the chamber until when conducting the comparison with the GP2Y sensors without regulated flows. Note that the convective flow regulated by the fan inside the AirAssure monitor might disturb the uniform distribution of particles in the chamber, possibly lead to some error in data analysis.

In the experiments, test particles were introduced into the chamber till the SidePak gave a mass concentration reading of around 5 mg/m^3, which is above the upper limit of the tested sensors as found in Section 4.1. The particle flow was discontinued and the system was allowed to equilibrate so that a uniform distribution of particle concentration and size distribution was obtained in the chamber. Due to particle precipitation and wall loss, the concentration of particles inside the chamber dropped gradually. Simultaneous measurements with the sensors, the SidePak, and the SMPS started when the mass concentration given by the SidePak was below 1 mg/m^3, which is slightly above the typical PM concentrations in highly polluted cities (Tiwari et al. 2013; Zhao et al. 2013; Guo et al. 2014). The whole process took approximately 2.5 h (Figure 2b), which was close to the gravitational precipitation time for a 1 μm (aerodynamic size) particle to drop from the top to the bottom of the chamber ($\sim$2.4 h). Hence, the evaluation results of the particle sensors were representative for PM_1 measurements.

3. ASSESSMENT ASPECTS

Six aspects of the sensor performance were studied in order to comprehensively understand their characteristics. Table 2 shows a brief summary of the experimental plan.

3.1. Linearity of Response

The linearity of response was assessed using the least-square regression and Reduced Major Axis (RMA) regression after plotting the outputs of the sensors against the SidePak measured particle mass concentrations. Particles were generated by burning incense (Sandalum Agarbathi Cones, Cycle Brand), which is reported to be an important source of indoor aerosol in certain countries (Cheng et al. 1995). The size distributions of the incense-generated particles as a function of time are displayed in Figure S1 in the online supplemental information (SI). Averaged outputs from the sensors on four sides of the chamber were used to evaluate their linearity. In the study, the particle mass concentrations measured by the SidePak were used as the independent variable, while the sensor outputs were reported as the dependent variables. Due to the existing uncertainty of the SidePak measured particle concentrations, the least-square regression may not be an adequate method to evaluate linearity. The RMA regression is specifically formulated to consider the errors in both the dependent and independent variables (Sokal and Rohlf 1981; McDonald 2009). Linear correlations, together with R^2 values, via the RMA regression and least-square regression were calculated. The RMA regression analysis was conducted with software designed by Bohonak and Linde (2004).

3.2. Precision of Measurements

The precision of the sensors was represented by their accuracy and repeatability of their measurements. The accuracy means the closeness between the measured results and the actual results, while the repeatability means the spread of the measured values (Petrozzi 2012). Due to the lack of a universal calibration curve for the three tested sensors, the linear correlations derived as described in Section 3.1 were used to evaluate sensor accuracy. Therefore, the accuracies of the sensors with less linearity became lower. At the same time, the accuracies of all three particle sensors became dependent on the accuracy of the SidePak, which does not necessarily provide the actual particle concentration due to instrument errors and the missing of the calibration factors. The repeatability of the sensors was evaluated by the variation of sensor outputs at similar particle concentrations. In the experiments, due to the difficulty in maintaining the particle concentrations at a constant level, different batches of measurements with the particle

TABLE 2
Experimental plan for the evaluation and calibration of the particle sensors PPD, DSM, and GP2Y

Test no.	Assessment aspect	Source of particles	Reference instruments
1	Linearity of response	Incense burning	SidePak, AirAssure
2	Concentration resolution	Incense burning	SidePak, AirAssure
3	Limit of detection	Incense burning	SidePak
4	Dependence on composition	Atomized NaCl, sucrose, and NH_4NO_3 particles	SidePak, SMPS
5	Sensitivity to particle size	Atomized PSL spheres with 300, 600, 900 nm	SidePak, SMPS
6	RH and temperature influence	Atomized NaCl particles	SidePak, SMPS

sensors were conducted, so that a series of sensor outputs was obtained corresponding to the same SidePak reported particle mass concentrations. The linear correlation derived in Section 4.1 was then applied to convert sensor outputs to particle concentrations. The standard deviations (σ) and the standard deviations relative to the SidePak measured particle concentrations were then calculated to evaluate the precision of measurements.

3.3. Limit of Detection

The limit of detection (LOD) is defined as the lowest limit that deviates significantly from the signal obtained from blank measurements. Similar quantifications of detection limits also exist, such as the limit of determination, limit of quantitation (LOQ), and limit of blank (Petrozzi 2012). In this study, the LOD was obtained with the widely used Kaiser and Specker (1956) method:

$$\mathrm{LOD} = 3\sigma_{\mathrm{blk}}/k \quad [1]$$

where σ_{blk} is the standard deviation at blank conditions maintained by filling the chamber with air cleaned by HEPA filters. k is the slope of the fitted line obtained from linearity experiments described in Section 4.1. Values of coefficients other than 3 before σ_{blk}/k were also used for other quantifications of detection limits: for example, the limit of determination uses 6, and the LOQ uses 10. The σ_{blk} was calculated based on a measurement time of 60 min, meaning that 120 samples have been collected for each of the sensors.

3.4. Dependence on Particle Composition

A sensor's performance depends on particle composition, since light scattering is influenced by the refractive index. This study used three types of particles, produced by atomizing NaCl, sucrose ($C_{12}H_{22}O_{11}$), and NH_4NO_3 aqueous solutions. To exclude the effect of particle size on the performance of the particle sensors, the concentrations of the solutions were controlled to ensure that generated particles had similar normalized size distributions (Figure S2 in the SI). After exiting the atomizer (Aerosol Generator 3076, TSI Inc.), particles passed through a custom-built diffusion dryer before entering the chamber. The different refractive indices of these three materials affected the performance of the particle sensors. The evolutions of particle size distributions during the measurements were found to be similar to that of the incense particles (Figure S1 in the SI), that is, the normalized size distributions remained the same, while the total particle concentration decreased. This property could exclude the effect of particle size change during the experiments. Due to the fact that the SidePak also measures particle concentrations with light scattering, reference concentrations were calculated from the size distributions obtained by the SMPS measurements. The outputs of the sensors, together with the readings of the SidePak were then compared with the mass concentrations calculated from size distributions.

3.5. Dependence on Particle Size

Light scattering is strongly dependent on particle size in both the Rayleigh regime and Mie regime. To assess this dependence, water solutions of polystyrene latex (PSL, Bangs Inc.) spheres were atomized to obtain particles with uniform diameters of 300 nm, 600 nm, and 900 nm, respectively. The mass concentrations of particles were calculated from the size distributions measured by the SMPS. The performance of the sensors and the SidePak were then evaluated by comparing the outputs with the mass concentrations calculated from the size distributions.

3.6. RH and Temperature Influence

RH values of 20%, 67%, 75%, and 90%, and temperatures of 5°C, 20°C, and 32°C were used to test the sensors. The RH and temperature were measured with a sensor probe (HMP60, Vaisala Inc., accuracy: ±3% in 0 to 90% RH, ±5% in 90 to 100% RH) and a type K thermocouple (OMEGA Inc., accuracy: ±2.2°C), respectively. The temperature was controlled by placing ice packs or heating tapes around the chamber. The RH was adjusted by flowing dry air through a deionized water bubbler and then into the chamber before the test. After the RH reached the set values, the feeding of water vapor was discontinued, and particles were introduced into the chamber. The decrease of RH was found to be less than 10% during the test. In this study, the particles were generated by atomizing NaCl aqueous solution. Again, similar normalized particle size distributions as a function of time were observed in the experiments, and hence the effect of particle size change during the experiments could be excluded.

4. RESULTS AND DISCUSSION

This section discusses the experimental results on assessing the particle sensors using the revised protocol provided by EPA 2013 Air Sensor Workshop.

4.1. Linearity of Response

When using the incense as the particle source, the response of the three sensors and the SidePak agreed well in the particle mass concentration range of 0–1000 $\mu g/m^3$ (Figures 3 and 4). Pairwise correlations among the instruments were higher than 0.78 (DSM2 against GP2Y1). To further evaluate the properties of the three sensors, their responses were plotted against the SidePak measured particle concentrations in Figure 4. Pairwise correlations between the outputs of the sensors and the SidePak measured particle concentrations were higher than 0.8914, as

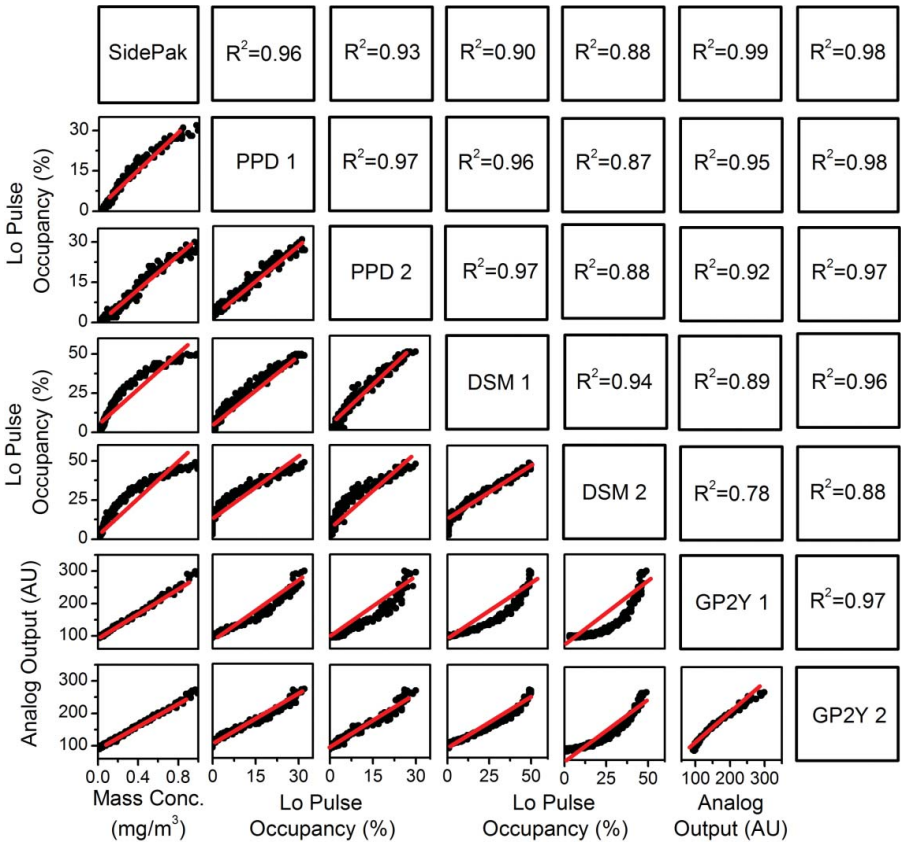

FIG. 3. Pairwise correlation among the three sensors and the SidePak during the 2.5 h measurement of the incense particles with a sampling interval of 30 s. Due to the limited space for plotting, two sensors of each type (PPD1, PPD2, DSM1, DSM2, GP2Y1, and GP2Y2) were chosen for comparison. The raw sensor outputs (Lo Pulse Occupancy and Analog Output) were used. R^2 values were calculated by the least-square regression.

indicated by the R^2 values calculated by the least-square regression (Figures 4a, b, d, e, g, and h). Given the low cost of these particle sensors, it will be worthwhile to apply these sensors to obtain local and real-time PM concentrations in polluted cities, where the daily upper limit of particle concentrations is around 600 μg/m^3, and the hourly upper limit of particle concentrations is higher than 1 mg/m^3 (Tiwari et al. 2013; Zhao et al. 2013; Guo et al. 2014). Among the three sensors, the GP2Y sensor gave the highest linearity with an R^2 value of 0.9838 for sensors of the same type on four sides of the chamber wall in one measurement, and 0.9831 for the same sensor on one side of the chamber wall in several measurements. The DSM sensors provided the lowest values of R^2, with 0.8914 for sensors of the same type, and 0.8921 for the same sensor.

It should be noted that the lower R^2 values given by the PPD and DSM sensors were mainly caused by the "curvature" at higher particle concentrations shown in Figures 4a, b, d, and e. A substantial enhancement in the linearity of the PPD and DSM sensors can be expected in smaller particle concentration ranges. For example, the PPD and DSM sensors gave R^2 values of 0.9496 and 0.9506, respectively, in the particle concentration range of 0–100 μg/m^3. For practical applications or enacting regulations on atmospheric particulate matter, these lower particle concentration ranges may be used (EPA 2013; MEP 2013).

In testing particle sensors of the same type, some deviated significantly from the others, although the linearity was still high (Figures 4a, d, and g, as indicated by the arrows). This systematic deviation could not be explained by the concentration fluctuations at the four sides of the chamber, as shown in Figure 2b. This result suggests that each sensor should be calibrated separately before being used in commercialized particle monitors, since this existing systematic error may significantly affect the particle concentrations reported by the sensors (e.g., the same analog output of 200 from a GP2Y sensor corresponded to a particle concentration ranging from 600 to 900 μg/m^3 in Figure 4g). The linearity of the same sensor was similar in each test (Figures 4b, e, and h), demonstrating the reliability of the sensor for repeated measurements, as discussed in Section 4.2. Figures 4c, f, and i shows the range of the particle concentrations in which sensors can be relied on. It was observed that the outputs of the three tested sensors became saturated at a concentration of around 4 mg/m^3 measured by the SidePak. Hence, the tested particle sensors are less applicable for measuring particle concentrations in highly polluted spaces, such as the outlet of stacks and construction sites.

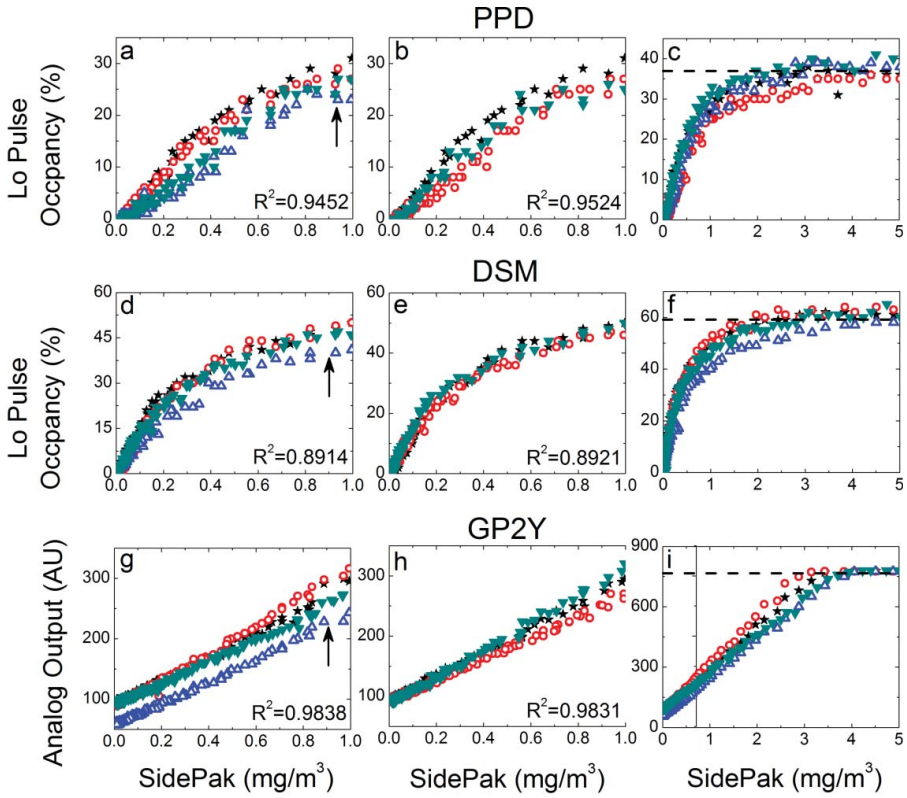

FIG. 4. Pairwise correlation between the sensor outputs and the SidePak data during the 2.5 h measurement of the incense particles with a sampling interval of 30 s: (a–c): PPD, (d–f): DSM, (g–i): GP2Y. (a), (d), (g): response of particle sensors of the same type in the concentration range of 0–1000 μg/m^3, different symbols represent the response of different sensors of the same type; (b), (e), (h): response of the same particle sensor in the particle concentration range of 0–1000 μg/m^3, different symbols represent the response of a same sensor for different batches of experiments; (c), (f), (i): response of particle sensors of the same type in the particle concentration range of 0–5000 μg/m^3. R^2 values were calculated by the least-square regression.

Table 3 gives the linear regression results of the three sensors using the least-square and RMA regression. The two regression methods yielded similar results, indicating a minimal influence of the variation of the SidePak measured particle concentrations. The least-square regression values in the particle concentration ranges of 0–100 μg/m^3 and 0–300 μg/m^3 were also tabulated, clearly showing the dependence of linearity on the choice of particle concentrations ranges. Note that the R^2 values obtained in this study are relatively larger than those calculated in previous studies on field calibration of the particle sensors (Holstius et al. 2014; Gao et al. 2015). This discrepancy may be due to variations in the material composition and size of the atmospheric particles in field calibrations, whereas the incense particles were the only particle source in the linearity test. Sections 4.4 and 4.5 elaborate the influence of particle composition and size on the performance of the particle sensors.

TABLE 3
Linear correlations between particle sensor outputs and SidePak measured particle concentrations in different ranges of particle concentrations (0–1000 μg/m^3, 0–100 μg/m^3, and 0–300 μg/m^3), calculated by the least squares and reduced major axis (RMA) regression methods

	Least squares (0–1000 μg/m^3)			RMA (0–1000 μg/m^3)			Least squares (0–100 μg/m^3)			Least squares (0–300 μg/m^3)		
Sensors	Intercept	Slope	R^2	Intercept	Slope	R^2	Intercept	Slope	R^2	Intercept	Slope	R^2
PPD	−0.353	33.6	0.9452	−0.481	34.3	0.9558	−0.806	47.1	0.9496	−1.05	43.4	0.9525
DSM	3.93	59.7	0.8914	3.34	63.2	0.8924	−0.469	159	0.9506	−0.0469	119	0.9755
GP2Y	91.1	196	0.9838	90.8	198	0.9831	94.2	190	0.9332	94.2	189	0.9746

Making modifications to the GP2Y sensor prototype could further enhance the linearity of response, as shown in Figure 5. R^2 value calculated by the lease-square method increased to 0.9961 for the AirAssure monitor. This improvement might be brought by regulated flow, which decreased the amount of erratically distributed particles staying in the light scattering region of the particle sensor. The specialized algorithm of the AirAssure might also flatten the fluctuating sensor outputs and provided results with higher linearity.

4.2. Precision of Measurements

Experimental results on the repeatability of the three tested sensors as measured by the standard deviation and relative standard deviation are plotted as a function of SidePak concentration in Figure 6. The standard deviations of the sensors varied from 15 μg/m^3 to 90 μg/m^3 for a concentration range of 0–1000 μg/m^3 (Figure 6a). Although the imprecision could also be partly attributed to the SidePak, the RMA regression calculated in Section 4.1 suggested a minimal influence of the SidePak's fluctuation. The DSM sensor demonstrated relatively constant and small values of standard deviation in the particle concentration range of 0–1000 μg/m^3, which can also be observed from the higher repeatability of the measurement in Figure 4e compared to other sensors. The PPD and the GP2Y sensors showed increased values of standard deviations at higher particle concentrations (Figure 6a), while the relative standard deviations of all the three tested sensors dropped as particle concentration increased (Figure 6b). The trend of increased relative standard deviation as concentration decreased indicates that the sensors are not very accurate for low concentration measurements (<200 μg/m^3). It should be noted that these standard deviations were calculated based on approximately 10 measurements due to constraints of the system used for the laboratory study. If the number of measurements were increased, it is anticipated that the uncertainty maybe lower. However, by averaging the data, the "real-time" information of the sensors may be lost. As in our system for testing incense combustion where the generated particle concentration decays rapidly in a sampling interval of 30 s, the averaged data over a longer period of time may not represent the actual particle concentration. Similar problems may be encountered when measuring fluctuating particle concentrations. In these situations, the high standard deviation of the sensor might cause a high uncertainty of the measurements. In this laboratory study, due to the considerable change of particle concentration in the sampling interval, the effect of averaging the measurements on the sensor performance was not investigated.

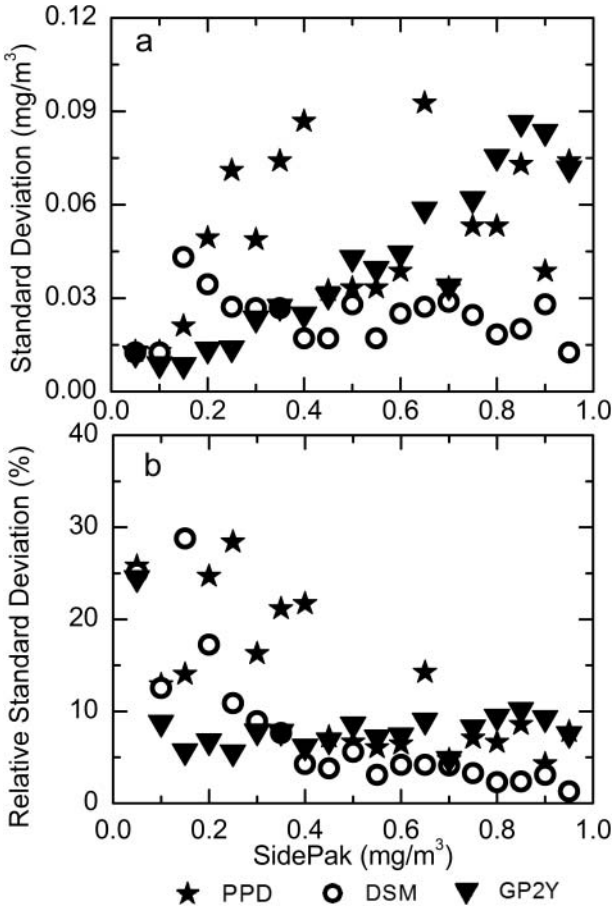

FIG. 6. (a) Standard deviations and (b) relative standard deviations of the sensor-measured particle concentrations under different SidePak-measured particle concentrations. The GP2Y sensors were tested without regulated convective flow.

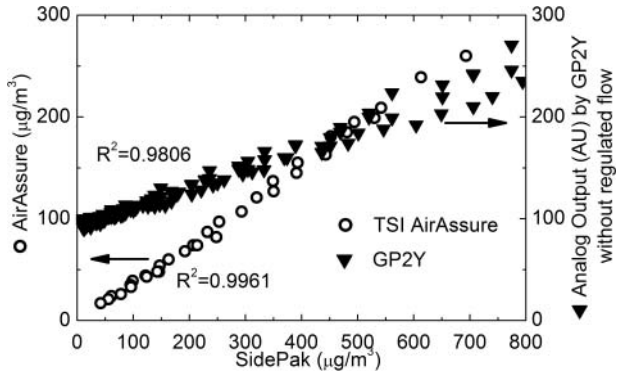

FIG. 5. Mass concentrations measured by the AirAssure monitor and analog outputs reported by the GP2Y sensor without regulated convective flow in mass concentration range of 0–800 μg/m^3. The experiment was conducted with the incense particles during a measurement time of around 2.5 h with a sampling interval of 30 s. Mass concentrations on the x-axis were measured with the SidePak.

In the applications of real-time measurements, these sensors can be utilized to locate hotspots for particle emissions in the ambient conditions, and to measure PM concentrations in non-ambient environments of interest, such as indoor areas and industrial plants. Furthermore, these particle sensors could serve as preliminary substitutes for more accurate instruments

in developing countries, where the atmospheric PM concentrations are high, and the commonly used accurate instruments are unaffordable. The AirAssure monitor reported particle mass concentrations with relatively higher repeatability, as shown in Figure 5, indicating the improvement of data quality after modifying the GP2Y sensor prototypes. Calculated standard deviations of the AirAssure monitor were below 10 $\mu g/m^3$ in the range of measurement between 0 and 300 $\mu g/m^3$. Note that the standard deviations of the particle sensors reflect the repeatability of the measurements, while precision is also described by the accuracy of the correlation between sensor outputs and particle concentrations. Since linear correlations of the three sensors in the particle concentration range of 0–1000 $\mu g/m^3$ were used in calculating particle concentrations, due to the low linearity of the DSM and PPD sensors as discussed above, the accuracy of the measurement was also negatively affected. Hence, depending on the specific properties of each type and model of the sensor, nonlinear correlations between the sensor output and the particle concentration are suggested to be calibrated to obtain more precise measurement results. For this study, simple second-order polynomial fittings could predict the response of the PPD and DSM sensors with much higher R^2 values. In the particle range of 0–1000 $\mu g/m^3$, the Lo Pulse Occupancy (LPO,%) of the PPD and DSM sensors could be fitted with equations:

$$\mathrm{LPO_{PPD}} = -17.8\,\mathrm{m}^2 + 47.7\,\mathrm{m} - 1.39 \text{ and} \quad [2]$$

$$\mathrm{LPO_{DSM}} = -75.3\,\mathrm{m}^2 + 118\,\mathrm{m} + 0.544, \quad [3]$$

with R^2 values of 0.9651 and 0.9798, respectively, where m is the mass concentration ($\mu g/m^3$) measured by the SidePak. The calculated R^2 values were much higher than those obtained from the linear regressions, and can be further improved by fitting the sensor outputs with higher orders of polynomial equations.

4.3. Limit of Detection

Table 4 lists the limits of detection (LOD), together with the values of σ_{blk} and k of the three tested sensors according to the calculation method introduced in Section 3.3. By using the k values obtained from the linear correlation in the concentration range of 0–1000 $\mu g/m^3$, the GP2Y sensor gave the highest LOD value of 30.2 $\mu g/m^3$. The LOD values of the PPD and the DSM sensors were relatively lower, with the PPD sensor showing the lowest LOD of 6.44 $\mu g/m^3$. Accordingly, the LOQ for the GP2Y sensor and the PPD sensor were 101 and 21.5 $\mu g/m^3$, respectively. Considering the higher gradient of the response of the PPD and DSM sensors in the lower particle concentration range, the LOD values of the two types of sensors would become smaller if linear correlations in lower particle concentration ranges were used. Table 4 also lists the LOD values of the PPD and DSM sensors using the k values calculated from the least-square regression in the particle concentration range of 0–100 $\mu g/m^3$, where lower LOD values of 4.59 $\mu g/m^3$ and 4.28 $\mu g/m^3$ were obtained.

4.4. Dependence on Particle Composition

The SidePak also uses light scattering to measure particle mass concentrations, which are affected by the particle composition and sizes. Hence, particle mass concentrations calculated from the size distributions of particles can provide higher accuracy for evaluating the sensor performance. As indicated in Figure S2 in the SI, the size distributions of the three types of generated particles were similar, and could be fitted by log-normal functions. The total mass concentration of the measured particles (m) can be calculated by using the method of moments (Hinds 1982):

$$m = \frac{\pi}{6} M_0 \exp\left(3\ln d_{pg} + \frac{9}{2}\ln^2(\sigma_g)\right), \quad [4]$$

where M_0, d_{pg}, and σ_g stand for the total number concentration, the geometric mean particle size, and the geometric standard deviation, which could be obtained through the curve fitting process.

The outputs of the particle sensors, together with the readings of the SidePak, were then plotted against the particle concentrations calculated from the size distributions (Figure 7). Due to the difficulty in generating highly concentrated sucrose particles, the performance of the sensors and the SidePak was

TABLE 4
Limits of detection of the three tested sensors using k values in different mass concentration ranges (0–1000 $\mu g/m^3$ and 0–100 $\mu g/m^3$). The GP2Y sensors were tested without regulated convective flow

Sensors	PPD	DSM	GP2Y
$3\sigma_{blk}$	0.216 (%)	0.680 (%)	5.11
k(0–1000 $\mu g/m^3$)	0.0336 (%×$m^3/\mu g$)	0.0597 (%×$m^3/\mu g$)	0.196 ($m^3/\mu g$)
LOD (0–1000 $\mu g/m^3$)	6.44 ($\mu g/m^3$)	11.4 ($\mu g/m^3$)	26.1 ($\mu g/m^3$)
k(0–100 $\mu g/m^3$)	0.0471 (%×$m^3/\mu g$)	0.159 (%×$m^3/\mu g$)	0.190 ($m^3/\mu g$)
LOD (0–100 $\mu g/m^3$)	4.59 ($\mu g/m^3$)	4.28 ($\mu g/m^3$)	26.9 ($\mu g/m^3$)

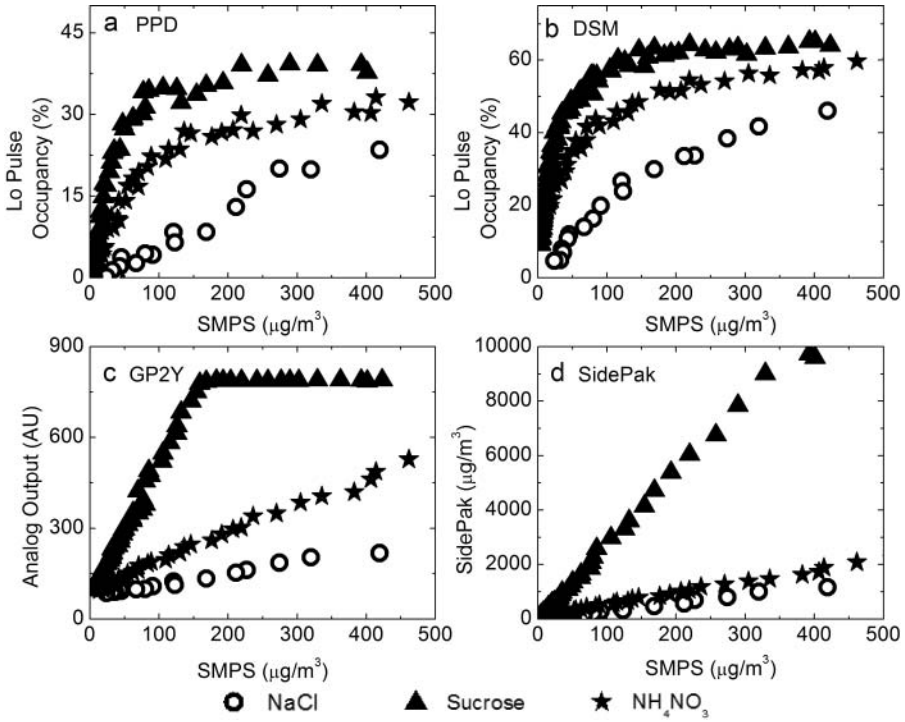

FIG. 7. Dependence of sensor performance on the composition of particles: (a) PPD, (b) DSM, (c) GP2Y, and (d) SidePak. The reference mass concentrations were calculated from the size distributions measured by the SMPS. The experiments were conducted with atomized NaCl, NH_4NO_3, and sucrose particles, each with a total measurement time of around 2 h with a sampling interval of 30 s. Note the different scales of *y*-axes.

evaluated in a mass concentration below 500 $\mu g/m^3$. It can be seen that the composition of the particles indeed affected the response of the particle sensors: the outputs increased by up to 10 times when measuring sucrose particles (the GP2Y sensor).

Moreover, different sensors and instruments responded differently when the composition of particles changed, as indicated by the magnitudes of the slopes in Figure 7. For example, the GP2Y sensors and the SidePak were more sensitive to the sucrose particles. As discussed by Molenar (2000), the variability of the refractive index of different materials accounts partly for the uncertainties when using light scattering to measure particle mass concentrations. The refractive index is the sum of a real and an imaginary component: $m = n - in'$, where n and n' are correlated with the magnitude of light scattering and light absorption, respectively. A higher proportion of light could be absorbed by organic compositions in particles, due to the energy storage in the vibration of carbon bonds, while inorganic materials are reported to absorb negligible radiation, that is, the imaginary term of the refractive index is close to zero. The phototransistor hence received less light in the test of sucrose particles, and so reported a higher mass concentration. This result implies that particle sensors may overestimate mass concentrations when measuring particles incorporating organic compositions. The outputs of the sensors measuring NaCl and NH_4NO_3 particles were also found to be different from each other, due to the different values of refractive indices. In this study, NH_4NO_3 was used to simulate the measurement of atmospheric particles in heavily polluted areas, since a large proportion of the inorganic contents of atmospheric particles is attributed to the reaction between NH_3 and HNO_3 (Jimenez et al. 2009; Guo et al. 2014; Seinfeld and Pandis 2012). The retained sensitivity at higher particle mass concentrations of NH_4NO_3 may promise the application of the three sensors in measuring particle concentrations in polluted ambient environments that contain mostly inorganic particles. However, for human health and exposure studies, particles with different contents may be measured. Due to the uniqueness of each device, a higher accuracy could be guaranteed if calibration factors were determined and applied for the materials being used.

4.5. Dependence on Particle Size

Figure 8 shows the dependence of sensor performance on the size of the tested particles, of which the size distributions are displayed in Figure S3 in the SI. The outputs of the particle sensors and the SidePak are plotted against particle mass concentrations calculated from the SMPS measured size distributions in the concentration below 500 $\mu g/m^3$. A higher concentration of 900 nm PSL particles could not be obtained, possibly due to the loss by impaction and interception during the transport of particles. Note that the mass concentrations reported by the SMPS might not accurately represent the actual values, because the narrow size

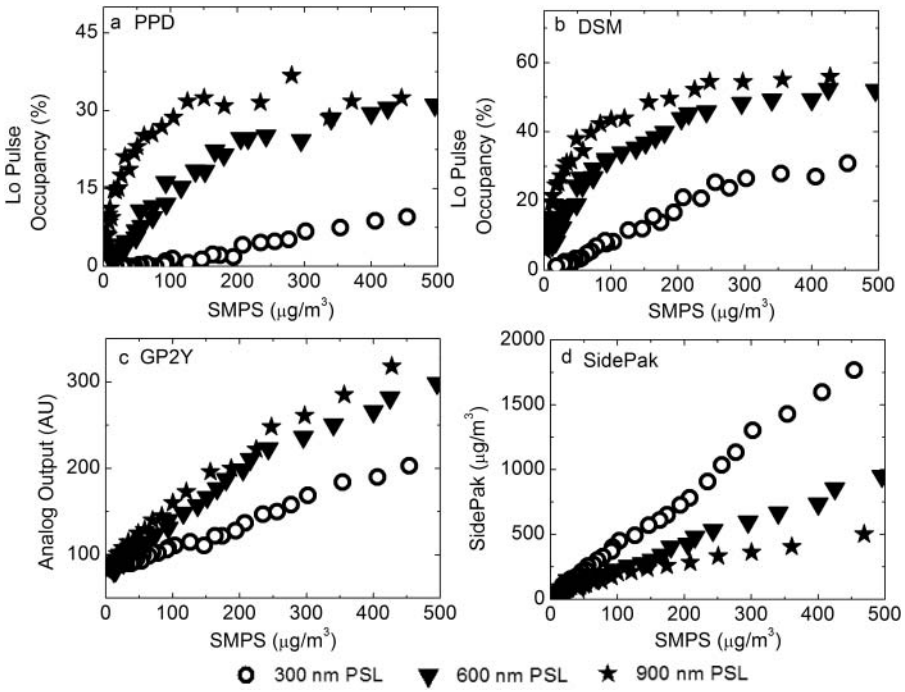

FIG. 8. Sensor performance for PSL particles with three sizes of 300, 600, and 900 nm, each during a measurement time of around 2 h with a sampling interval of 30 s: (a) PPD, (b) DSM, (c) GP2Y, and (d) SidePak. The reference mass concentrations were calculated from the size distributions measured by the SMPS. Note the different scales of *y*-axes.

distributions of the PSL particles may not be regarded as a constant value in the transfer function of the DMA (Stolzenburg and McMurry 2008). Different characteristics were observed among the sensors and the SidePak. Under the same mass concentrations, the outputs of the sensors became higher as particle sizes increased from 300 nm to 900 nm, while the SidePak reported the highest particle concentration for the smallest particles (300 nm). Further observation on the response of the particle sensors indicated that the GP2Y sensor was more sensitive to smaller particles, while the PPD and DSM sensors were more sensitive to larger particles. These properties can be attributed to the type of the irradiated light used in the instruments. For safe handling and reduced cost, infrared radiation between 870 and 940 nm was used in the particle sensors, while the SidePak uses a laser with a wavelength of 670 nm for the light scattering of particles. Although the light scattering of the sensors and the SidePak all fall into the Mie Regime, the relative magnitude of the particle size and the wavelength of the radiation determined that the light scattering in the particle sensors is closer to the Rayleigh regime.

In the experiments, as particle size increased, the response of the particle sensors was enhanced for the same mass concentration (Figures 8a–c), which could be explained as follows. For the same mass concentration of monodisperse particles, $N_{TOT}d_p^3$ remains a constant, where N_{TOT} is the total number concentration of particles with a size ofd_p. The scattered light (I_{scat}) has the form of

$$I_{scat} = I_0 N_{TOT} Q_{scat} \frac{\pi}{4} d_p^2, \quad [5]$$

where I_0 is the incident light, and Q_{scat} is the scattering coefficient. Since the light scattering for the sensors was closer to the Rayleigh regime, for a simple estimation, Q_{scat} was assumed to be proportional to d_p^4 (Friedlander 2000). Note that this correlation might overestimate the light scattering coefficient in the Mie regime. The scattered light intensity is therefore proportional to $N_{TOT}d_p^6$, and further proportional to d_p^3 under the same mass concentration. Because of the correlation that $I_{scat} = Kd_p^3$, where K is a constant, more light was lost due to the extinction of larger particles, less light was received by the phototransistor, and higher concentrations were reported. Based on this result, the particle sensors may underestimate the particle mass concentrations for smaller particles. On the contrary, the SidePak reported a reverse trend for the influence of particle sizes, possibly due to the fluctuations in the light scattering coefficient in the Mie regime, which affected the amount of light lost in the sensor and received by the transistor.

4.6. RH and Temperature Influence

Relative humidity affected the performance of the particle sensors in several ways. First, similar to organic compositions, water absorbs infrared radiation and can cause an overestimate

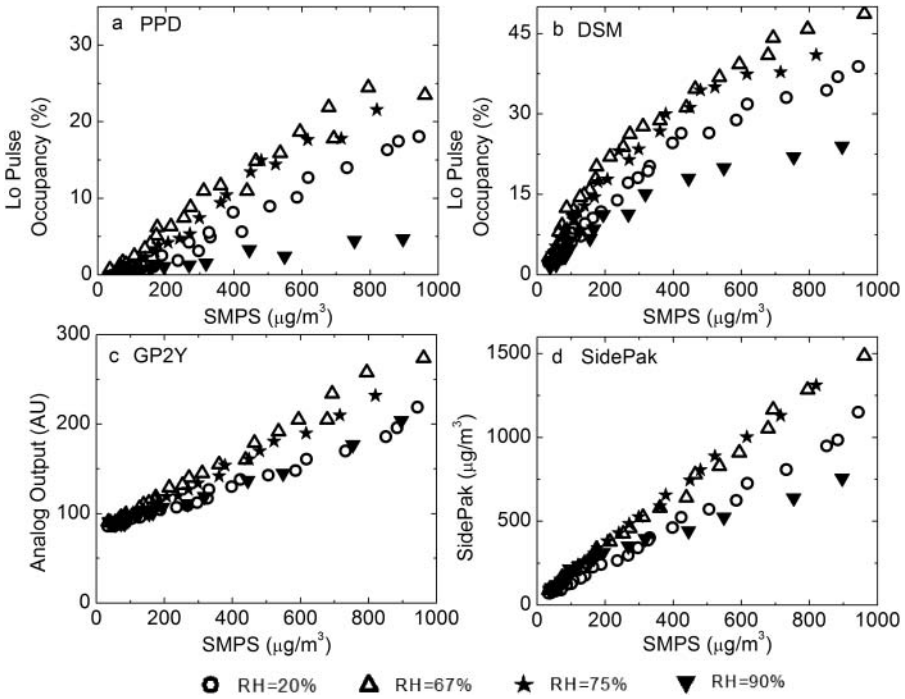

FIG. 9. Performance of particle sensors under various relative humidity values (20% to 90%), each with a measurement time of around 2.5 h with a sampling interval of 30 s: (a) PPD, (b) DSM, (c) GP2Y, and (d) SidePak. The reference mass concentrations were calculated from the size distributions measured by the SMPS. Note the different scales of *y*-axes.

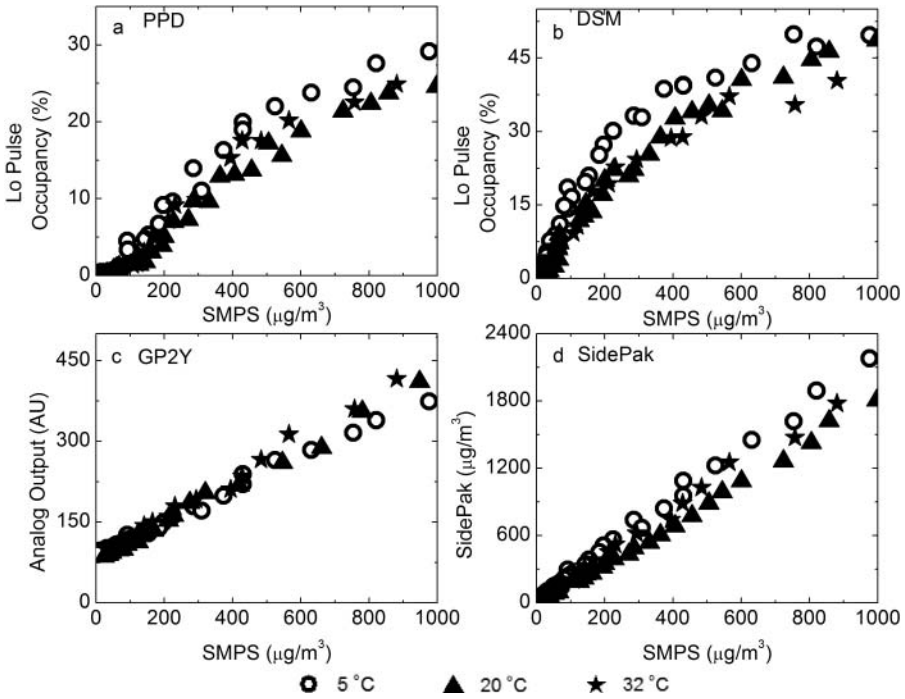

FIG. 10. Performance of particle sensors at different temperatures of 5°C, 20°C, and 32°C, each with a measurement time of around 2.5 h with a sampling interval of 30 s: (a) PPD, (b) DSM, (c) GP2Y, and (d) SidePak. The reference mass concentrations were calculated from the size distributions measured by the SMPS. Note the different scales of *y*-axes.

TABLE 5
Summary of the characteristics of the particle sensors PPD, DSM, and GP2Y

Assessment aspects	PPD	DSM	GP2Y
Linearity of response[#]	Medium	Low	High
Precision of measurement			
Accuracy[*]	Medium	Low	High
Repeatability	Low	High	Medium
Limit of detection	Low	Low	High
Dependence on composition	High	High	High
Sensitivity to particle size	High	High	High
RH influence	High	High	High
Temperature influence	Minimal	Minimal	Minimal

[#]The linearity of response is evaluated based on the R^2 values in the particle concentration range of 0–1000 $\mu g/m^3$.
*Accuracy is based on the correlations calculated from linear regression methods. Nonlinear correlations are suggested in order to enhance the accuracy of the measurement.

of particle mass concentrations due to the reduced light intensity received by the phototransistor. Second, highly concentrated water vapor may lead to a failure of the circuits of the particle sensors and result in biased measurement results. Third, the usage of SMPS data as references may not be applicable under high RHs, since the sheath flow inside the DMA may dry the particles and cause an underestimate of particle concentrations measured by the SMPS. As shown in Figure 9, similar trends in the performance of the particle sensors and the SidePak were observed as RH altered. For the same particle mass concentration, the outputs of the sensors and the SidePak first increased, and then dropped as RH increased. This result may be a comprehensive effect of the factors mentioned above, clearly showing the dependence of sensor performance on RH values.

Compared to relative humidity, temperature had negligible effects on the three particle sensors and the SidePak in the temperature range from 5°C to 32°C, as shown in Figure 10, because theoretically, light scattering and absorption are independent of temperature. However, extreme temperatures of the environment may affect the reported particle concentrations, since the flow rate of the updraft of particles in the PPD and the DSM sensors is determined by the temperature difference between the thermal resistor and the environment.

5. CONCLUSIONS

This work comprehensively evaluated three low-cost light scattering particle sensors. A brief summary of the characteristics of the three sensors was compiled, and the advantages of each sensor were determined (Table 5). Throughout the experiments, the GP2Y1010AU0F (GP2Y) sensor demonstrated the highest linearity in comparison to measurements by the SidePak. The data quality of the GP2Y sensors could be further enhanced by modifying the flow system and the algorithm for calculating particle concentrations, as indicated by the improvement in the response of an AirAssure monitor. The PPD42NS (PPD) and the DSM501A (DSM) sensors had relatively lower limits of detections than the GP2Y sensors. Some common characteristics were observed, such as the saturated outputs under high particle concentrations of around 4 mg/m^3, high dependence on the composition and size of particles, and minimal dependence on temperature.

While the relative standard deviation increased with decrease in concentration (these sensors may not be as accurate as more complicated and expensive measurement devices in clean environments), these low cost particle sensors demonstrated the ability to report particle concentrations with relatively high linearity and moderate repeatability. In addition, the uncertainty of the measurement can be further reduced by averaging the measurements over longer periods of time. The compact size and low cost of the sensors favor their wide application in tracking air quality in developing countries and heavily polluted areas, where the demand for monitoring particulate matter is especially urgent for the sake of public health. Large data sets obtained by the sensor network will make amenable applications of concepts of "big data" to improve the air quality.

ACKNOWLEDGMENTS

The authors thank TSI for providing the prototype of the AirAssure $PM_{2.5}$ Indoor Air Quality Monitor for testing. Yang Wang thanks Drs. Yungang Wang at ERM, Siqin He, and Qisheng Ou at University of Minnesota for the helpful discussion.

FUNDING

This work was partially supported by a grant from National Science Foundation (NSF CBET 1437933).

SUPPLEMENTAL MATERIAL

Supplemental data for this article can be accessed on the publisher's website.

REFERENCES

Biswas, P., and Wu, C.-Y. (2005). Nanoparticles and the Environment. *J. Air Waste Manage. Assoc.*, 55:708–746.

Bohonak, A. J., and Linde, K. V. D. (2004). Reduced Major Axis Regression. Available at: http://www.kimvdlinde.com/professional/rma.html.

Cao, J., Chow, J. C., Lee, F. S., and Watson, J. G..(2013). Evolution of PM2. 5 Measurements and Standards in the US and Future Perspectives for China. *Aerosol Air Qual. Res.*, 13:1197–1211.

Cheng, Y. S., Bechtold, W. E., Yu, C. C., and Hung, I. F. (1995). Incense Smoke: Characterization and Dynamics in Indoor Environments. *Aerosol Sci. Tech.*, 23(3):271–281.

Chong, C.-Y., and Kumar, S. P. (2003) Sensor Networks: Evolution, Opportunities, and Challenges. *Proc. IEEE*, 91:1247–1256.

Chowdhury, Z., Edwards, R. D., Johnson, M., Shields, K. N., Allen, T., Canuz, E., and Smith, K. R. (2007). An Inexpensive Light-Scattering Particle Monitor: Field Validation. *J. Environ. Monit.*, 9:1099–1106.

Edwards, R., Smith, K. R., Kirby, B., Allen, T., Litton, C. D., and Hering, S. (2006). An Inexpensive Dual-Chamber Particle Monitor: Laboratory Characterization. *J. Air Waste Manag. Assoc.*, 56:789–799.

EPA, US (2013). 40 CFR Parts 50, 51, 52, 53, and 58-National Ambient Air Quality Standards for Particulate Matter: Final Rule. *Federal Register*, 78:3086–3286.

Friedlander, S. K. (2000). *Smoke, Dust, and Haze*. Oxford University Press, New York.

Gao, M., Cao, J., and Seto, E. (2015). A Distributed Network of Low-Cost Continuous Reading Sensors to Measure Spatiotemporal Variations of PM2. 5 in Xi'an, China. *Environ. Pollut.*, 199:56–65.

Guo, S., Hu, M., Zamora, M. L., Peng, J., Shang, D., Zheng, J., Du, Z., Wu, Z., Shao, M., and Zeng, L. (2014). Elucidating Severe Urban Haze Formation in China. *Proc. Natl. Acad. Sci.*, 111(49):17373–17378.

Hagler, G., Solomon, P., and Hunt, S. (2014). *New Technology for Low-Cost, Real-Time Air Monitoring*. EM (Air Waste Manage. Assoc.), 1, Pittsburg, PA.

Hinds, W. C. (1982). *Aerosol Technology: Properties, Behavior, and Measurement of Airborne Particles*. John Wiley & Sons, New York.

Holstius, D., Pillarisetti, A., Smith, K., and Seto, E. (2014). Field Calibrations of a Low-Cost Aerosol Sensor at a Regulatory Monitoring Site in California. *Atmos. Meas. Tech. Discuss.*, 7:605–632.

Huang, R.-J., Zhang, Y., Bozzetti, C., Ho, K.-F., Cao, J.-J., Han, Y., Daellenbach, K. R., Slowik, J. G., Platt, S. M., and Canonaco, F. (2014). High Secondary Aerosol Contribution to Particulate Pollution During Haze Events in China. *Nature*, 514:218–222.

Jimenez, J., Canagaratna, M., Donahue, N., Prevot, A., Zhang, Q., Kroll, J., DeCarlo, P., Allan, J., Coe, H., and Ng, N. (2009). Evolution of Organic Aerosols in the Atmosphere. *Science*, 326:1525–1529.

Kaiser, H., and Specker, H. (1956). Bewertung und Vergleich von Analysenverfahren. *Fresenius' J. Anal. Chem.*, 149:46–66.

Karlsson, H. L., Gustafsson, J., Cronholm, P., and Möller, L. (2009). Size-Dependent Toxicity of Metal Oxide Particles—A Comparison Between Nano-and Micrometer Size. *Toxicol. Lett.*, 188:112–118.

Knutson, E., and Whitby, K. (1975). Aerosol Classification by Electric Mobility: Apparatus, Theory, and Applications. *J. Aerosol Sci.*, 6:443–451.

Leavey, A., Fu, Y., Sha, M., Kutta, A., Lu, C., Wang, W., Drake, B., Chen, Y., and Biswas, P. (2015). Air Quality Metrics and Wireless Technology to Maximize the Energy Efficiency of HVAC in a Working Auditorium. *Build. Environ.*, 85:287–297.

Litton, C. D., Smith, K. R., Edwards, R., and Allen, T. (2004). Combined Optical and Ionization Measurement Techniques for Inexpensive Characterization of Micrometer and Submicrometer Aerosols. *Aerosol Sci. Tech.*, 38:1054–1062.

Long, R., Beaver, M., Williams, R., Kronmiller, K., and Garvey, S. (2014). *Procedures and Concepts of EPA's Ongoing Sensor Evaluation Efforts*. EM (Air Waste Manage. Assoc.), 8, Pittsburg, PA.

McDonald, J. H. (2009). *Handbook of Biological Statistics*. Sparky House Publishing, Baltimore, Maryland, USA.

MEP (2013). *Environmental Laws*. Chinese Ministry of Environmental Protection (MEP) of the People's Republic of China, Beijing, China.

Molenar, J. V. (2000). Theoretical Analysis of PM2.5 Mass Measurements by Nephelometry. PM2000: Particulate Matter and Health, Specialty Conference, January 24-28, 2000, Charleston, SC, Air & Waste Management Association.

Mulholland, G. W., and Liu, B. Y. (1980). Response of Smoke Detectors to Monodisperse Aerosols. *J. Res. Natl. Bureau Standards*, 85:223–238.

Nafis, C. (2012). Air Quality Monitoring. Available at: http://www.howmuchsnow.com/arduino/airquality/.

Olivares, G., Longley, L., and Coulson, G. (2012). Development of a Low-Cost Device for Observing Indoor Particle Levels Associated with Source Activities in the Home. International Society of Exposure Science (ISES), Seattle, WA.

Petrozzi, S. (2012). *Practical Instrumental Analysis: Methods, Quality Assurance and Laboratory Management*, John Wiley & Sons, Singapore.

Phalen, R., Cuddihy, R., Fisher, G., Moss, O., Schlesinger, R., Swift, D., and Yeh, H.-C. (1991). Main Features of the Proposed NCRP Respiratory Tract Model. *Radiat. Prot. Dosim.*, 38:179–184.

Rajasegarar, S., Zhang, P., Zhou, Y., Karunasekera, S., Leckie, C., and Palaniswami, M. (2014). High Resolution Spatio-Temporal Monitoring of Air Pollutants Using Wireless Sensor Networks. In *Intelligent Sensors, Sensor Networks and Information Processing (ISSNIP), 2014 IEEE Ninth International Conference, IEEE*, pp. 1–6, Singapore.

Sahu, M., Peipert, J., Singhal, V., Yadama, G. N., and Biswas, P. (2011). Evaluation of Mass and Surface Area Concentration of Particle Emissions and Development of Emissions Indices for Cookstoves in Rural India. *Environ. Sci. Technol.*, 45:2428–2434.

Schubert, E. (2006). *Light-Emitting Diodes*. Cambridge University Press, Cambridge, UK.

Seinfeld, J. H., and Pandis, S. N. (2012). *Atmospheric Chemistry and Physics: From Air Pollution to Climate Change*. 2nd Ed. John Wiley & Sons, Hoboken, NJ.

Sokal, R. R., and Rohlf, F. J. (1981). *Correlation and Multiple and Curvilinear Regression, Biometry*. WH Freeman & Co, New York, pp. 561–690.

Spinelle, L., Gerboles, M., and Aleixandre, M. (2013). *Protocol of Evaluation and Calibration of Low-Cost Gas Sensors for the Monitoring of Air Pollution*. Publication Office of the European Union, Luxembourg, EUR 26112.

Stocker, T., Qin, D., Plattner, G., Tignor, M., Allen, S., Boschung, J., Nauels, A., Xia, Y., Bex, B., and Midgley, B. (2013). IPCC, 2013: Climate Change 2013: The Physical Science Basis. Contribution of Working Group I to the Fifth Assessment Report of the Intergovernmental Panel on Climate Change.

Stolzenburg, M. R., and McMurry, P. H. (2008). Equations Governing Single and Tandem DMA Configurations and a New Lognormal Approximation to the Transfer Function. *Aerosol Sci. Tech.*, 42:421–432.

Tiwari, S., Srivastava, A., Bisht, D., Parmita, P., Srivastava, M. K., and Attri, S. (2013). Diurnal and Seasonal Variations of Black Carbon and PM 2.5 over New Delhi, India: Influence of Meteorology. *Atmos. Res.*, 125:50–62.

US Embassy (2015). Air Quality Data. Available at: http://beijing.usembassy-china.org.cn/070109air.html, http://newdelhi.usembassy.gov/airqualitydataemb.html.

Wang, S. C., and Flagan, R. C. (1990). Scanning Electrical Mobility Spectrometer. *Aerosol Sci. Tech.*, 13:230–240.

Weekly, K., Rim, D., Zhang, L., Bayen, A. M., Nazaroff, W. W., and Spanos, C. J. (2013). Low-Cost Coarse Airborne Particulate Matter Sensing for Indoor Occupancy Detection. *IEEE CASE*, 2013:32–37.

Zhao, X., Zhao, P., Xu, J., Meng, W., Pu, W., Dong, F., He, D., and Shi, Q. (2013). Analysis of a Winter Regional Haze Event and Its Formation Mechanism in the North China Plain. *Atmos. Chem. Phys.*, 13:5685–5696.